UNIVERSITY OF BIRMINGHAM

University of Birmingham
Research at Birmingham

Benefits of mechatronically guided vehicles on railway track switches

Farhat, Nabilah; Ward, Christopher P.; Dixon, Roger; Goodall, Roger M.

Link to publication on Research at Birmingham portal

Benefits of mechatronically-guided vehicles on railway track switches

Nabilah Farhat, Christopher P. Ward, Roger Dixon, Roger M. Goodall

Abstract

Conventional rail vehicles struggle to optimally satisfy the different suspension requirements for various track profiles, such as on a straight track with stochastic irregularities, curved track or switches and crossings (S&C), whereas mechatronically-guided railway vehicles promise a large advantage over conventional vehicles in terms of reduced wheel-rail wear, improved guidance and opening new possibilities in vehicle architecture. Previous research in this area has looked into guidance and steering using MBS models of mechatronic rail vehicles of three different mechanical configurations - secondary yaw control (SYC), actuated solid-axle wheelset (ASW) and driven independently-rotating wheelsets (DIRW). The DIRW vehicle showed the best performance in terms of reduced wear and minimal flange contact and is therefore chosen in this paper for studying the behaviour of mechatronically-guided rail vehicles on conventional S&Cs.

In the work presented here, a mechatronic vehicle with the DIRW configuration is run on moderate and high speed track switches. The longer term motivation is to perform the switching function from on-board the vehicle as opposed to from the track as is done conventionally. As a first step towards this, the mechatronic vehicle model is compared against a conventional rail vehicle model on two track scenarios - a moderate speed C type switch and a high speed H switch. A multi-body simulation software is used to produce a high fidelity model of an active rail vehicle with independently-rotating wheelsets (IRWs) where each wheel has an integrated 'wheelmotor'.

This work demonstrates the theory that mechatronic rail vehicles could be used on conventional S&Cs. The results show that the mechatronic vehicle gives a significant reduction in wear, reduced flange contact and improved ride quality on the through-routes of both moderate and high speed switches. On the diverging routes, the controller can be tuned to achieve minimal flange contact and improved ride quality at the expense of higher creep forces and wear.

Introduction

Railway track switches enabled the development of a rail network with multiple routes. Although track switches make up less than 0.1% of the complete rail network, more than 10% of total maintenance costs is spent towards constantly replacing or re-profiling worn switches [Capacity for Rail (2015)]. They represent safety-critical assets that can cause widespread disruption of rail services in the event of a failure. The consequent cost of delayed or cancelled services can quickly build up making switch failures a very expensive problem [Bemment et al. (2017)].

The basic mechanism of track switches has not changed since their invention more than 200 years ago. Figure 1 shows the layout of a conventional track switch. The stock rails are fixed securely while the ends of the switch rails displace laterally to form the selected route for the rail vehicle. This mechanism involves a rapid change in contact patch from stock rail to switch rail at the toe. This is also the case at crossings where the wheel has to travel across the gap designed to provide flange clearance.

There has been a considerable effort in industry to make the load transition from stock rail to switch rail smoother. This includes the introduction of moveable crossing nose [Lindner (1974)], especially for high speed turnouts with
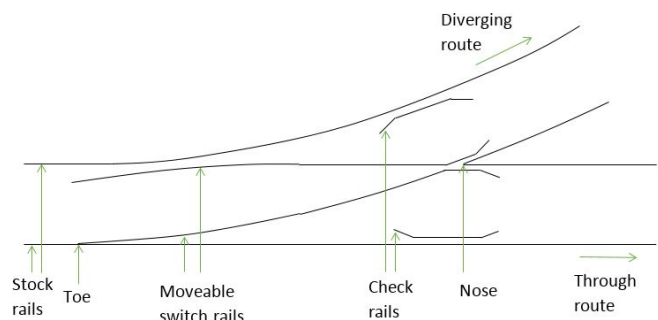
Figure 1. Typical track switch layout

a shallower divergence angle and a consequently larger gap. Other efforts include flange bearing crossings which support a wheel from under the flange to allow rail vehicles to ride on their wheel flange [Caterpillar (2018)]. Despite these improvements, track switches still remain a largely

Corresponding author:
Nabilah Farhat, Wolfson School of Mechanical, Electrical and Manufacturing Engineering, Loughborough University, LE11 3TU, UK
Email: n.farhat@lboro.ac.uk

mechanical concept that rely on the switch rails moving laterally to close the gap between itself and the adjacent rail on one side while maintaining a gap on the opposite side for the flange to pass through.

Vehicle-based switching proposes to perform switching from on-board the vehicle. The motivation is to have a purely passive track switch, which does not rely on any moving parts and the switching is done entirely from the vehicle instead. Vehicle-based switching has probably been conceptualised since the invention of railways with "Rivington's self-acting railway switches" being one of the earliest appearances in literature in [Rivington (1838)]. The underside of the vehicle has an inclined plane which pushes a bell crank which moves the switch blades into position. Although it is largely a mechanical concept, it represents a shift in controlling the switching from track to vehicle, although the switch action itself remains part of the track.

More recently, with developments in electronics, vehicle-based switching has been envisioned as a control application where the wheels can be individually controlled with torque-controlled motors relying on sensors. One such proposition is that of [Koseki et al. (2000)] where the wheels on a wheelset can be individually-driven to generate the required creep forces to produce the necessary yaw angle. Another idea is to have a permanent magnet on the underside of the vehicle and electromagnetic rails for both through and diverging routes [Bushko et al. (2000)]. When the vehicle goes over the switch it is attracted to either the rails for the through or the diverging route depending on which of the electromagnets is turned on.

The work presented in this paper studies an active steering mechanism with a motor on each wheel. The wheels can rotate independently as they are not rigidly connected by a solid axle. Such 'wheelmotors' have been designed by a company called Stored Energy Technology (SET) and retrofitted on a Blackpool tram [SET Ltd. (2013)]. The motors are torque-controlled and use wheelset lateral displacement as a feedback signal which is difficult to measure in practice. However, in the work presented here, the idea is to establish the benefits of the active vehicle, assuming ideal feedback signals are available. This is considered as a preliminary study with a view that the practicalities of sensing need to be addressed at a later stage. This paper compares the performance of an active vehicle running on a moderate and a high speed railway track switch against that of a conventional vehicle. The results presented here indicate that the active vehicles could be used with conventional track switches to reduce wear. So this study considers the possibility of a mixed traffic of mechatronic and conventional vehicles on railway track switches. Ultimately, if the entire traffic was mechatronic, switches could be redesigned to optimise such vehicles and maximise benefits. This longer term vision of vehicle-based switching could ultimately allow active steering on a purely passive track switch that has no moving parts as has been proposed previously [Ward et al. (2013)]. This means that switch reliability would be improved as the turnout has a permanent position and does not require locking or detection mechanisms. They would also not need to be controlled from an external operations centre, reducing the human factor elements of track switch operation.

In the following sections, the track switch modelling and the active vehicle modelling in Simpack are described. The active steering mechanism and the controller design process are also explained in detail. Finally, the performance of the active vehicle is assessed in terms of Tγ values which indicate wear levels and lateral displacement of the front wheelset of the vehicle. Switches also suffer from plastic deformation and rolling contact fatigue (RCF) which is well-established for solid-axle wheelsets. RCF crack initiation depends on the forces generated at the wheel-rail contact, which will be predominantly lateral for IRWs and hence largely different. However, in order to give some indication of RCF damage using the proposed mechatronic vehicle, the thresholds verified for solid-axle wheelsets are used in this paper.

Track switch model

The switch geometry considered consists of a straight 'through-route' and a 'diverging-route' to the left of the straight track. The stock, switch and check rail profiles used are CEN56 E1, CEN54 E1A1 and CEN33 C1 respectively. The stock rail profile is described in detail in [Standards (2017)] and that of the switch rail is given in [Standards (2006)]. The check rail profile and its relationship with the running rail is described in the Network Rail Track Design Handbook [Rail (2010)].

Two types of track switches are modelled to study the active vehicle at different maximum allowable speeds. The running rails are inclined by 1:20 in both switch models. A C switch is chosen because it is the most commonly occurring switch on the UK mainline. The machining of the switch rail at different distances from the toe is described in detail in the RE/PW/1602 B drawings. The crossing nose profile detail is given in RE/PW/1769 drawing. A C switch is usually located at or near stations due to its relatively tight radius of $\approx$245 m on the diverging route. The maximum allowable speed on this switch is 25 mph.

A high speed H type turnout is chosen to study the behaviour at speeds of 90 mph. This switch has a curve radius of $\approx$3000 m on the diverging route and consequently a shallow diverging angle of 1 in 32. This makes the gap at the crossing over 4 m long which necessitates the use of a swingnose crossing. The swingnose geometry details are given in the Track Switch Handbook. The machining of the switch rail in this is similar to that of a C switch but spread across a longer planing length.

Table 1 lists some of the main dimensions and the rail profiles used in the different elements of each switch. A track gauge of 1432 mm is maintained throughout.

As the rail profiles are constantly changing at switches and crossings, the Simpack modelling of an S&C involves specifying the rail profile at different cross sections along the forward running direction of the rail vehicle. The cross sections are generated from CAD models of the switches which are developed from the rail profile geometries described in British Standards and the RE/PW drawings. MATLAB is used to slice the CAD model to generate the cross-sectional profiles. The profiles are specified using a Cartesian coordinate system where the origin is at the top centre of the rail head as shown in Figure 2.

Table 1. Table listing key C and H turnout details. Note that IP is the intersection point where the two rails cross just before the crossing gap.

Dimension	Switch type	
	C	H
Toe to IP length (mm)	24877	89693
Radius of curvature (mm)	245767	3000716
Divergence angle (1 in -)	9.25	32.365
Gap length (mm)	148	4118
Maximum turnout speed (mph)	25	90

Figure 2. Rail wheel profile axes

(a) Switch toe

(b) Change in contact from stock to switch rail

(c) Gap

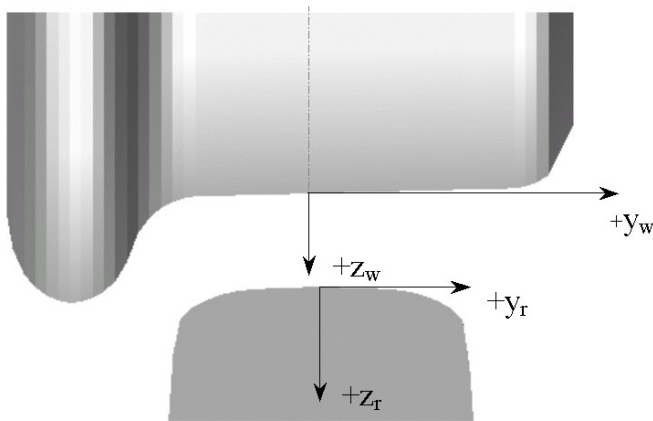**(d)** Crossing nose

Figure 3. Different cross sections in the Simpack C switch model

The z axis is positive in the downward direction and the y axis is positive towards the right. The third axis is the s axis along the direction of the track, which is also the forward running direction of the rail vehicle. The contours are specified in Simpack in the form of files which specify the y,z coordinates at a particular value of s. Figure 3 illustrates some of these cross-sectional profiles and different points along the C switch. Simpack performs an interpolation between consecutive cross sections to form a continuous rail. Figure 3a shows the profile at the switch toe and 3b shows the profile where the contact patch shifts from the stock rail to switch rail. Figures 3c and 3d illustrate the profiles at the crossing gap and nose respectively. For a left-handed switch, these profiles occur on the left rail for the through-route and on the right rail for the diverging-route. The opposite rail has a stock rail profile with the check rail appearing at the crossing.

Active vehicle model

The vehicle model is also developed in Simpack. This does not require forming the equations of motion from first principles as this is already done in the software for each of the individual elements that make up the full vehicle model. The Simpack model takes into account non-linearities in the rail-wheel profile and deadbands in some suspension components making it a high fidelity model of a real rail vehicle [Polach et al. (2006)].

The vehicle model is based on a passenger vehicle with two bogies and two wheelsets on each bogie. The intention is that the active vehicle requires the most straightforward modifications to a 'conventional' bogie as a first step towards an incremental solution that could be implemented on more
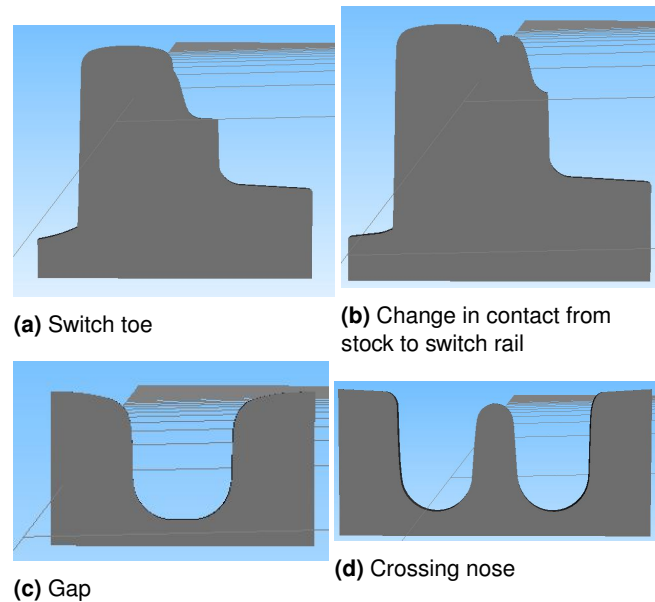
radical vehicles. A standard S1002 wheel profile is used for all the wheels. The wheels on the same axle can rotate independently of each other due to the absence of a rigid connection between them. However, this removes the self-guidance of solid-axle wheelsets which needs to be provided through control. Each wheel experiences longitudinal, lateral and spin creepages. Creepage or creep forces are generated when wheels don't have a pure rolling motion and instead slide against the rails. In IRWs, the wheels are able to roll with minimal slip thus producing negligible longitudinal creep forces.
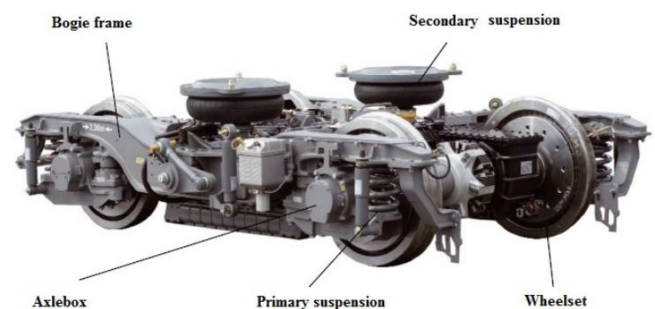
Figure 4. Components of a railway vehicle suspension [Yusof et al. (2011)]

Figure 4 shows the components of a railway vehicle suspension. The primary suspension between each wheelset and bogie consists of lateral, longitudinal and vertical springs. A damper is also connected in parallel to the lateral spring. The secondary suspension between each bogie and the vehicle body has shear stiffnesses in x,y and z directions and rotational stiffnesses in the roll and pitch directions. The secondary suspension also provides stiffness and damping in the vertical, lateral and yaw modes. The vertical damping in the primary suspension, lateral and yaw damping in the secondary suspensions are non-linear functions of relative velocity with deadband regions.

The stiffnesses, damping coefficients of the different suspension elements in the primary and secondary suspension and the vehicle parameters are given in Table 2. The mass and inertia of different bodies and the stiffness and damping of the suspension components in the model are chosen to represent a typical modern rail vehicle [Goodall and Ward (2015)]. The primary longitudinal stiffness of the active vehicle is lower than that required to stabilise a conventional vehicle to reduce motor torque required to generate an overall wheelset yaw moment. The value given in Table 2 is that of a conventional passive vehicle at speeds less than 30 m/s. The stiffness is reduced to 3.14 MN/m for the active vehicle on the C switch to lower the actuation torque required. The reduction in longitudinal stiffness allows the control mechanism to provide the stability without needing to overcome high stiffnesses. On the H switch, the vehicle speed is 40 m/s which necessitates a stiffer suspension. The stiffness is increased to 20.14 MN/m for the active vehicle and to 40.14 MN/m for the conventional vehicle running on the H switch, which is typical of high-speed trains [Wickens (2003)].

Table 2. Simpack vehicle parameters for a passive vehicle at speeds upto 30 m/s.

Primary suspension element	Value	Units
longitudinal parallel stiffness	3.14×10^7	N/m
lateral parallel stiffness	6.5×10^6	N/m
lateral parallel damping	6×10^5	Ns/m
vertical parallel stiffness	5.22×10^6	N/m
stiffness of vertical damper	6×10^5	N/m
Secondary suspension element	Value	Units
longitudinal shear stiffness	1.6×10^5	N/m
lateral shear stiffness	1.6×10^5	N/m
vertical stiffness	4.3×10^5	N/m
roll bending stiffness	1.05×10^4	Nm/rad
pitch bending stiffness	1.05×10^4	Nm/rad
stiffness of vertical damper	6×10^6	N/m
vertical damping	2.5×10^4	Ns/m
lateral stiffness	1×10^6	N/m
yaw stiffness	3.75×10^5	N/m
Key vehicle parameters	Value	Units
Vehicle body mass	20000	kg
Bogie mass	2615	kg
Wheelset mass	1200	kg
Half vehicle body length	11.2	m
Bogie semi-wheelbase	1.28	m
Half gauge width	0.75	m
Axlebox lateral semi-spacing	1	m
Wheel rolling radius	0.46	m

Figure 5 illustrates the plan view of half a rail vehicle with driven independently-rotating wheelsets (DIRW). Although, the motor is drawn separately from the wheel for the purpose of visual clarity, in reality, they are integrated into one unit. The DIRW mechanism is chosen from studying different active steering mechanisms because it shows the best performance on a straight track with stochastics and on a curved track with 1 m/s^2 cant deficiency. The other active steering mechanisms studied are the Secondary Yaw
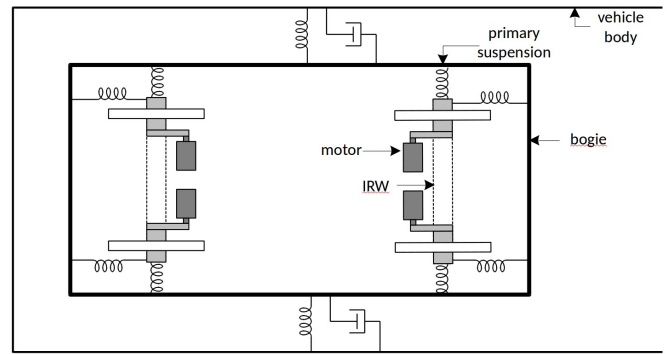

Figure 5. Configuration of a vehicle with driven independently-rotating wheelsets

Control (SYC) [Braghin et al. (2006)] and Actuated Solid-axle Wheelset (ASW) [Pearson et al. (2004)]. In the SYC mechanism, the control is at the secondary suspension level and balances the lateral creep forces on two axles on the same bogie by applying a yaw torque to the entire bogie. The ASW mechanism applies the yaw torque directly to the wheelset and aims to achieve pure rolling by controlling longitudinal creep forces. The energy dissipated in the wheel-rail contact patch is used to give an indication of wear and is called Tγ [Burstow (2012)]. The Tγ value of the DIRW vehicle was $\approx$20% of the SYC and $\approx$50% of the ASW vehicle on the curved track scenario. On the straight track simulations, the Tγ value of the DIRW vehicle was $\approx$15% of the SYC and $\approx$97% of the ASW vehicle [Farhat et al. (2018)].

The active steering mechanism involves using a 'wheel-motor' which is a mechanical integration of a wheel and a traction motor, instead of a conventional wheel. The torque supplied to each wheelmotor is controlled using a proportional integral plus [Young et al. (1987)] controller which uses the wheelset lateral displacement as the feedback signal. A PIP controller was chosen as it gave a better performance on straight and curved track profiles than classical proportional integral (PI) or phase advance (PA) controller. The torque supplied to the two wheels on a single wheelset are equal and opposite of each other. In this work, the motor torque is controlled rather than the speed as controlling the speed of the motors creates a virtual electronic axle having the characteristics of a solid-axle wheelset including kinematic instability [Mei and Goodall (2003)]. Torque-controlled motors affect the rotational acceleration of the wheels which results in different angular positions. The objective is that the differential torque will result in a net wheelset yaw angle to minimise the wheel-rail lateral displacement.

Controller design

In order to design the controllers, a linear model was necessary to analyse the frequency response of the system. This is achieved by performing system identification from the input torque to the output wheelset lateral displacement. System identification is chosen for two reasons. Firstly, this method could be extended to a full scale vehicle when designing control algorithms, so is preferred for its ease of applicability. Secondly, a simple model derived from first principles, did not show a good enough correlation to the

non-linear Simpack model. This could be attributed to the fact that a simpler model does not consider all degrees of freedom and assumes constant wheel conicity amongst many other simplifications.

Once the controller is designed, it is applied to the non-linear Simpack model using co-simulation. Figure 6 illustrates an overview of the co-simulation modelling environment where MATLAB/ Simulink runs in parallel with Simpack exchanging signals to close the control loop.
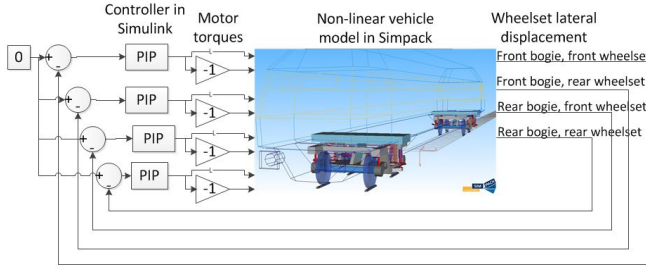

Figure 6. Co-simulation overview

All of the estimated models are ARX (autoregressive exogenous) models which have the following general form

$$A(z)y(k) = B(z)u(k - n) + e(k) \qquad (1)$$

where u(k) is the system inputs, y(k) is the system outputs, e(k) is the system disturbance, n is the system delay, A(z) and B(z) are the polynomials as a function of the delay operator z^{-1}.

For applying system identification the rail vehicle is run on a straight track with no stochastic disturbances and a small motor torque is applied to the front wheelset of the front bogie to excite the system dynamics. The input torque is a pulse with an amplitude of 1000 Nm and a small width of 0.25 s to accentuate the higher frequencies to get a good model estimation. The amplitude is chosen to be high enough to excite the system while maintaining minimal flange contact in order that the wheel-rail contact non-linearities can be assumed to be negligible. The vehicle speed is 11 m/s which is the maximum allowable speed through a C switch. The output is the wheelset lateral displacement. Each axle is considered as an independent single-input single-output (SISO) model where the input is the motor torque and the output is the wheelset lateral displacement. However, such SISO system identification assumes that each wheelset is decoupled from the others, which is not strictly true. In reality, the cross-coupling means that it is a multiple-input multiple output (MIMO) system with maximum coupling occurring between two wheelsets on the same bogie. However in this instance, a controller based on the SISO model works because the gain and phase margins accommodate for this level of uncertainty. So only a SISO model was used because of its lower order and ease of implementation. The estimated model is seventh order and has the following transfer function.

$$G(z) = \frac{-3.8 \times 10^{-10}z^6 - 3.5 \times 10^{-10}z^5 + 7.9 \times 10^{-10}z^4}{z^7 - 2.7z^6 + 2.3z^5}$$

$$\frac{-2.6 \times 10^{-10}z^3 + 1.9 \times 10^{-10}z^2 - 2.1 \times 10^{-10}z}{-0.4z^4 + 0.1z^3 - 0.4z^2}$$

$$\frac{+1.8 \times 10^{-10}}{+0.1z + 0.1} \qquad (2)$$

The estimated response has an R^2 metric of 91.58%. This is considered be good enough for a linear 'design' model which can be used to perform frequency analysis. Figure 7 shows the input torque, the output wheelset lateral displacement from the Simpack model and estimated ARX model and the error between them.
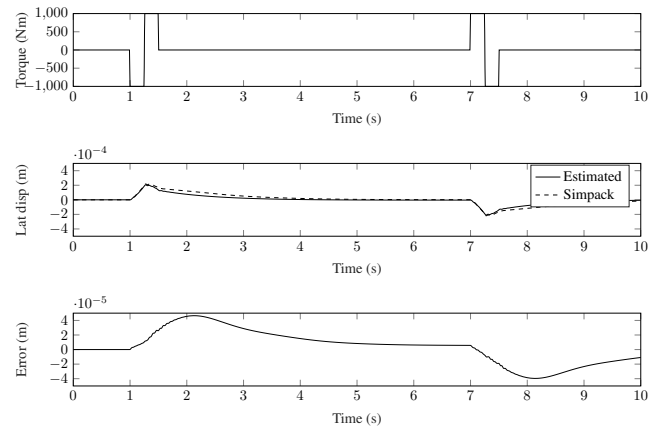

Figure 7. System identification applied to the DIRW vehicle model

For the frequency response, a gain margin (GM) greater than 6 dB and a phase margin (PM) greater than 60 degrees are commonly accepted to be large enough to accommodate for variations in plant dynamics or track disturbances [Dorf and Bishop (2008)]. The controllers designed must be able to cope with parametric uncertainties and non-linearities in the Simpack model as will be the case in application.

In the time domain, the following indicators are used to compare the performance of the DIRW vehicle against the conventional passive solid-axle vehicle model.

Tγ is the contact patch frictional energy, calculated as $T\gamma = F_x\epsilon_x + F_y\epsilon_y$ where F_x ,F_y are the longitudinal and lateral creep forces and ϵ_x, ϵ_y are the longitudinal and lateral creepages respectively. These values are indicative of wheel-rail wear. $T\gamma$ values have also been used to give an indication of rolling contact fatigue (RCF) crack initiation Burstow (2011). For solid-axle wheelsets, a value of 15 J/m is considered to be the threshold below which the frictional energy is insufficient to initiate RCF. At values above 175 J/m the rails get worn out due to the excessive energy and the wear is considered to be the dominant form of damage instead of crack initiation.

δ**-y** , wheelset lateral displacement with respect to the track centreline should be less than 6 mm to have minimum flange contact to maintain the wheel-rail non-linearities to a minimum.

$\ddot{y}_v$, car body lateral acceleration. The maximum allowable acceleration is 1 m/s^2 to maintain ride quality standards [Standards (2009)].

PIP controller

The PIP control system requires a non-minimal state space (NMSS) representation of a linear, discrete-time transfer function [Young et al. (1987)]. In the NMSS form, all the states depend on the present and past inputs and outputs of the system. Therefore they are directly measurable unlike a state-space form which may require observers for unmeasurable states.

An nth order single-input single-output (SISO) system in discrete-time can be expressed as

$$y(k) = \frac{B(z^{-1})}{A(z^{-1})} u(k) \tag{3}$$

where z^{-1} is the delay operator and B and A denote the numerator and denominator of the transfer function such that

$$A(z^{-1}) = 1 + a_1 z^{-1} + ... + a_n z^{-n}$$

$$B(z^{-1}) = b_1 z^{-1} + b_2 z^{-2} + ... + b_m z^{-m}$$

The NMSS form is expressed using the following equations

$$x(k) = Fx(k-1) + gu(k-1) + dy_d(k) \tag{4}$$

$$y(k) = Hx(k) \tag{5}$$

where k is the discrete-time variable, y_d is the command input and,

$$F = \begin{bmatrix} -a_1 & ... & -a_{n-1} & -a_n & b_2 & ... & b_{m-1} & b_m & 0 \\ 1 & ... & 0 & 0 & 0 & ... & 0 & 0 & 0 \\ \vdots & & \vdots & \vdots & \vdots & & \vdots & \vdots & \vdots \\ 0 & ... & 1 & 0 & 0 & ... & 0 & 0 & 0 \\ 0 & ... & 0 & 0 & 0 & ... & 0 & 0 & 0 \\ 0 & ... & 0 & 0 & 1 & ... & 0 & 0 & 0 \\ \vdots & & \vdots & \vdots & \vdots & & \vdots & \vdots & \vdots \\ 0 & ... & 0 & 0 & 0 & ... & 1 & 0 & 0 \\ a_1 & ... & a_{n-1} & a_n & -b_2 & ... & -b_{m-1} & -b_m & 1 \end{bmatrix}$$

$$g = \begin{bmatrix} b_1 \\ 0 \\ \vdots \\ 0 \\ 1 \\ 0 \\ \vdots \\ 0 \\ -b_1 \end{bmatrix} \quad d = \begin{bmatrix} 0 \\ 0 \\ \vdots \\ 0 \\ 0 \\ 0 \\ \vdots \\ 0 \\ 1 \end{bmatrix}$$

$$H = \begin{bmatrix} 1 & ... & 0 & 0 & 0 & ... & 0 & 0 & 0 \end{bmatrix}$$

The PIP control law resulting from the NMSS model is of the usual state-variable feedback form $u(k) = -kx(k)$. The F,g,d,H matrices depend only on the past inputs and outputs and not on any internal states. For a first order system with one sample time delay and one parameter in the numerator

polynomial, the PIP controller takes the form of a classical PI controller. For more complex systems, the PI element is retained and additional derivative action is provided through feedback from the higher order terms.

The gain matrix k is calculated using the 'dlqr' function in MATLAB which minimises the LQ cost function. Q is a diagonal matrix with weighting factors W_y, W_u and W_z which are tuned to achieve the desired frequency response and closed loop performance. W_y affects the response to the disturbance, W_u applies a weighting to the control torque and W_z governs the speed of the response. The weighting factors are selected heuristically to achieve the GM and PM requirements.

Figure 8 shows the open loop frequency response with and without the PIP controller. The uncompensated open loop response is from the motor torque in kNm to the wheelset lateral displacement in millimeters. The uncompensated open loop system has a GM of 29.1 dB and a PM of 63.1 degrees. The PIP controller gain matrix k is calculated by minimising the cost function with the weightings $W_y = 1 \times 10^{-3}$, $W_u = 1 \times 10^{-6}$ and $W_z = 2 \times 10^6$.

$$k = 1 \times 10^9 \quad [\text{-0.7} \quad 1.2 \quad \text{-0.4} \quad \text{-0.1} \quad \text{-0.2} \quad 0.1 \quad ...$$
$$0.1 \quad 0.0 \quad \text{-0.0} \quad \text{-0.0} \quad 0.0 \quad \text{-0.0} \quad ...$$
$$0.0 \quad \text{-0.0} \quad 0.0]$$

With the selected weightings on the PIP controller, the GM is reduced to 24.1 dB and the PM is 60.3 degrees. The closed loop system bandwidth is 6.12 Hz.
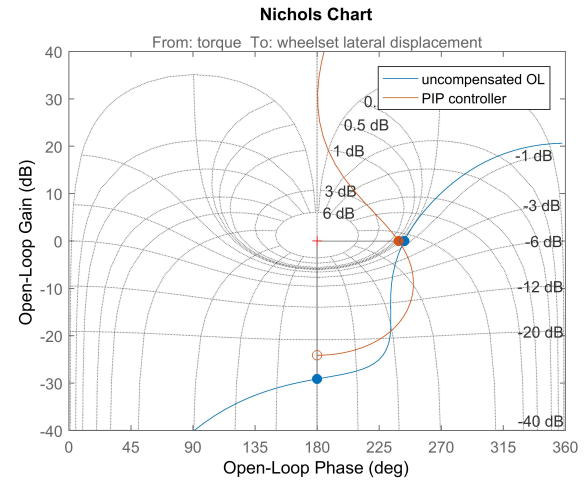

Figure 8. Nichols plot for PIP controller design.

Results

C switch simulations

Figure 9 shows the lateral displacements of the front and rear wheelsets with respect to the track centre-line on the through route of a C switch. At the switch toe, the lateral displacement of the DIRW wheelsets are much lower than that of the passive vehicle. At the nose, although the initial displacement is similar, the DIRW vehicle guidance responds quicker than the passive vehicle. This improvement in performance can also be seen from the T_γ values in Table 3 which are reduced to less than a quarter of the passive vehicle. The car body lateral acceleration is similar to that of the passive vehicle as shown in Figure 10.
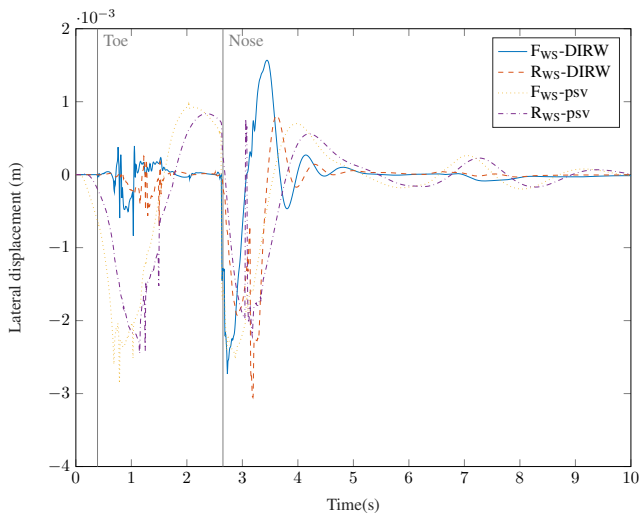
Figure 9. Wheelset lateral displacement on the through route of a C switch at v=11 m/s. The notations F_{WS}, R_{WS} and psv used in the graph labels mean 'front wheelset', 'rear wheelset' and 'passive' respectively.
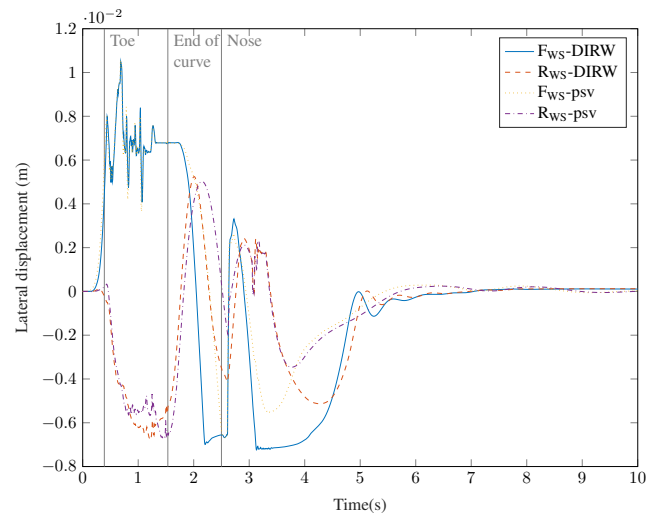

Figure 11. Wheelset lateral displacement on the diverging route of a C switch at v=11 m/s. The notations F_{WS}, R_{WS} and psv used in the graph labels mean 'front wheelset', 'rear wheelset' and 'passive' respectively.
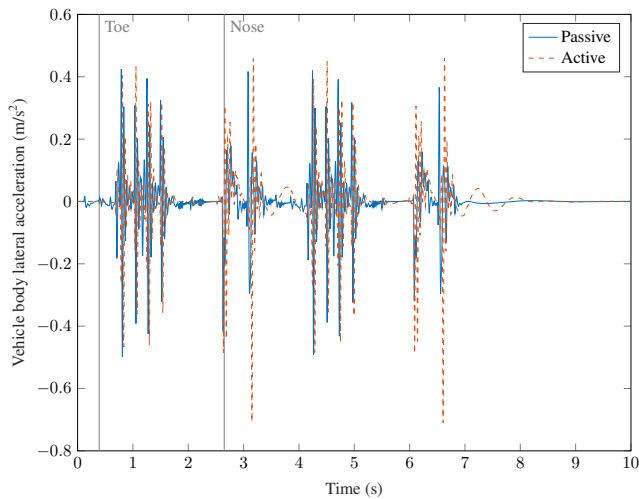

Figure 10. Vehicle body lateral acceleration on the through route of a C switch at v=11 m/s. The notations 'Active' and 'Passive' used in the graph labels mean the DIRW and conventional vehicles respectively.

Figure 12. Vehicle body lateral acceleration on the diverging route of a C switch at v=11 m/s. The notations 'Active' and 'Passive' used in the graph labels mean the DIRW and conventional vehicles respectively.
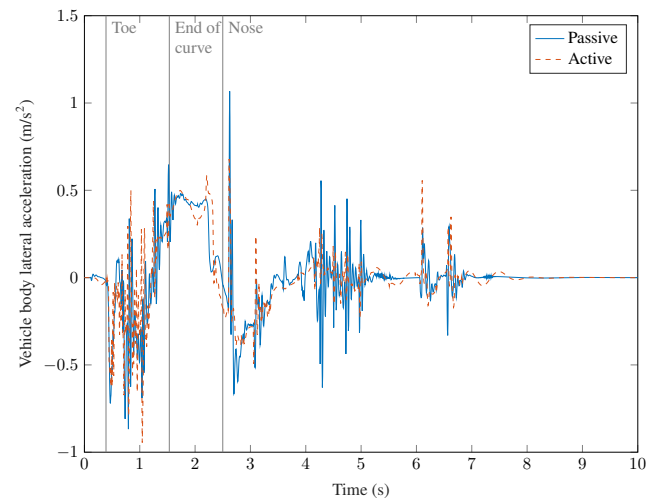
Table 3. $T\gamma$ values in J/m on the through route of a C switch.

	Passive	DIRW
Front bogie front WS	0.1639	0.1084
Front bogie rear WS	1.4347	0.7098
Rear bogie front WS	1.1965	0.0438
Rear bogie rear WS	1.6476	0.2387
Total $T\gamma$ on all WSs	4.4427	1.1007
Percentage of passive	100	24.78

Table 4. $T\gamma$ values in J/m on the diverging route of a C switch. The values in bold are those above the RCF threshold.

	Passive	DIRW
Front bogie front WS	**22.2665**	**30.6318**
Front bogie rear WS	8.5979	4.2829
Rear bogie front WS	**25.0218**	3.7758
Rear bogie rear WS	8.6362	6.0754
Total $T\gamma$ on all WSs	64.5224	44.7659
Percentage of passive	100	69.38

The diverging route has a tight curve radius where both vehicles make flange contact. The DIRW vehicle gives a very similar performance to the passive vehicle in terms of lateral displacement as shown in Figure 11. The wear is marginally better than the passive vehicle as indicated by the T_γ values in Table 4. The DIRW vehicle body acceleration is lesser than that of the passive vehicle at the switch nose, but is otherwise similar as shown in Figure 12.

In order to assess the running safety of the DIRW vehicle compared to the passive vehicle, the derailment coefficient graphs for each of the wheels were analysed. The derailment coefficient (Y/Q) is the ratio of the lateral and vertical forces at the wheel-rail interface and gives an indication of flange climb derailment. In the diverging route of the C switch, the wheelsets maintain flange contact for a greater distance

than in any of the other switch scenarios under consideration due to the fairly tight curve radius. Hence only the results for this scenario have been provided. The front wheelset of the vehicle experiences the maximum flange contact and generates the highest lateral creep forces compared to the other wheelsets. The right wheel is the flanging wheel in this instance because the switch under consideration has a left-handed turnout. Figure 13 shows the Y/Q graph for the right (flanging) wheel of the front wheelset of the active DIRW vehicle compared to the passive vehicle.
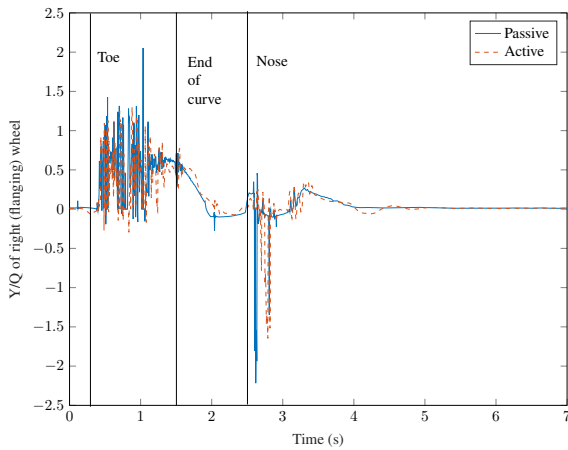

Figure 13. Y/Q of the right wheel of the front wheelset on the diverging route of a C switch. The notations 'Active' and 'Passive' used in the graph labels mean the DIRW and conventional vehicles respectively.

From the figure it can be seen that the responses for the passive and DIRW vehicle models are fairly comparable, so the active vehicle is not performing any worse than the passive vehicle in terms of running safety. Moreover, both vehicles are within recommended derailment coefficient levels [Wu and Wilson (2006)].

H switch simulations

On the through-route of the H switch, the lateral displacement of the DIRW vehicle is smaller than that of the passive case as shown in Figure 14. The vehicle body acceleration is also lower as shown in Figure 15. However the longitudinal creep forces are slightly higher resulting in a higher T_γ value as listed in Table 5. The values under 'DIRW 1' column are the results from maintaining the same controller gains as in the C switch. The controller could be re-tuned to trade-off a higher lateral displacement with smaller creep forces. This would necessitate gain scheduling for different switches.

With lower design weightings of W_y=0.001, W_u=0.0001 and W_z=200000, the gain and phase margins are increased to 41.4 dB and 61.7 degrees respectively. This results in a longer settling time for the wheelset lateral displacement as shown in Figure 16, but this is not a problem as the maximum values are still quite small. The T_γ values are significantly lower than the passive vehicle as listed in the 'DIRW 2' values in Table 5. The car body lateral acceleration is also smaller than that of the passive vehicle as shown in Figure 17. This shows that the controller could be re-tuned to reduce the
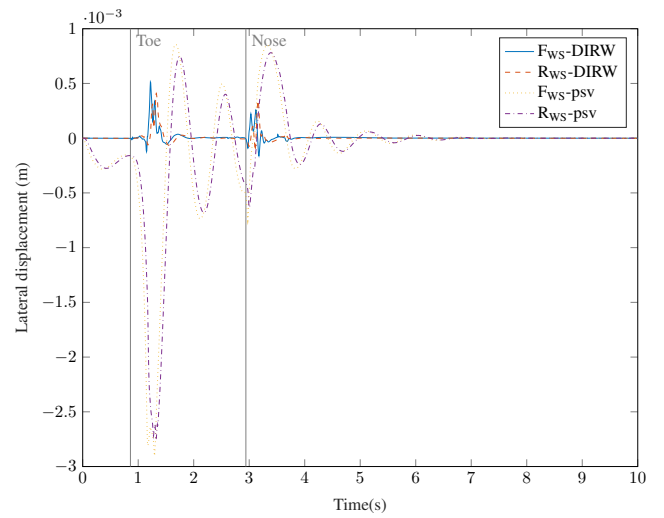

Figure 14. Wheelset lateral displacement on the through route of a H switch at v=40 m/s with the 'DIRW 1' controller. The notations F_{WS}, R_{WS} and psv used in the graph labels mean 'front wheelset', 'rear wheelset' and 'passive' respectively.
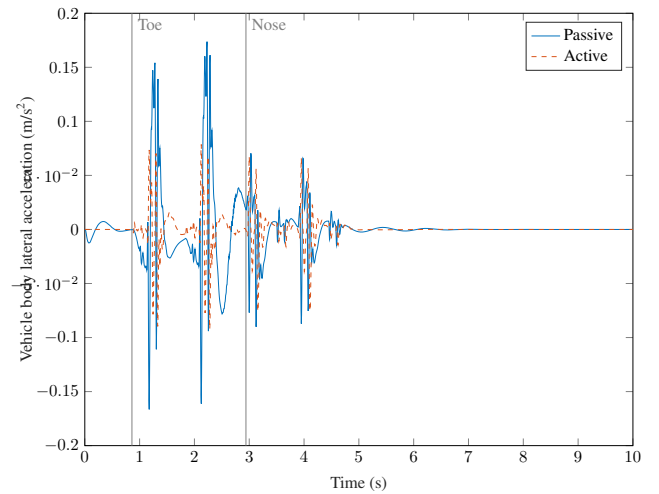

Figure 15. Vehicle body lateral acceleration on the through route of a H switch at v=40 m/s with the 'DIRW 1' controller. The notations 'Active' and 'Passive' used in the graph labels mean the DIRW and conventional vehicles respectively.

creep forces and resultant wear while not having any adverse effect on the wheelset lateral displacement or the ride quality.

Table 5. T_γ values in J/m on the through route of a H switch. The values under 'DIRW 1' column are obtained from simulations with higher controller gains than that in 'DIRW 2' column

	Passive	DIRW 1	DIRW 2
Front bogie front WS	0.03	0.06	0.0233
Front bogie rear WS	0.0663	0.0908	0.0150
Rear bogie front WS	0.0329	0.0567	0.0230
Rear bogie rear WS	0.0805	0.0873	0.0148
Total T_γ on all WSs	0.2097	0.2948	0.0761
Percentage of passive	100	140.58	36.29

On the diverging-route of the H switch, only the passive vehicle makes flange contact on the curve radius as shown in Figure 18. These results are from using the 'DIRW 1'
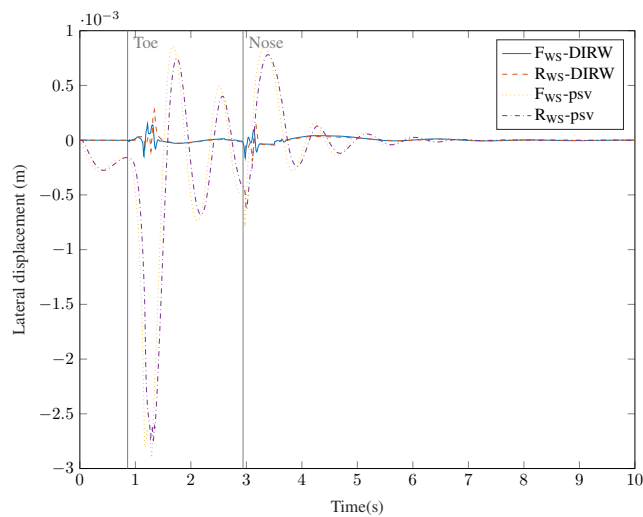
Figure 16. Wheelset lateral displacement on the through route of a H switch at v=40 m/s with the 'DIRW 2' controller. The notations F_{WS}, R_{WS} and psv used in the graph labels mean 'front wheelset', 'rear wheelset' and 'passive' respectively.
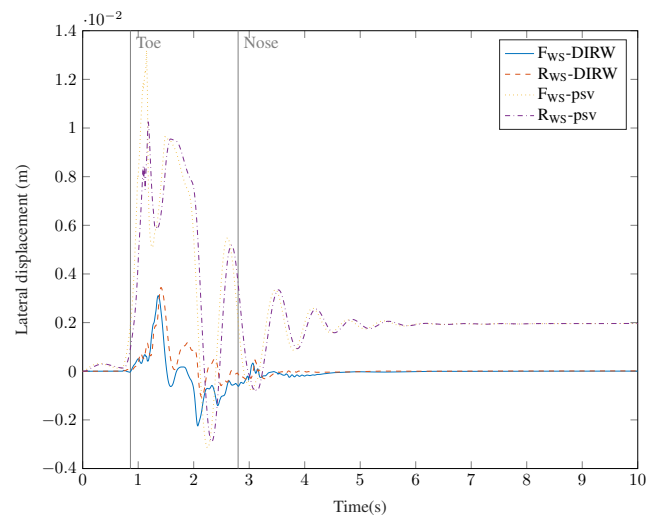

Figure 18. Wheelset lateral displacement on the diverging route of a H switch at v=40 m/s with the 'DIRW 1' controller. The notations F_{WS}, R_{WS} and psv used in the graph labels mean 'front wheelset', 'rear wheelset' and 'passive' respectively.
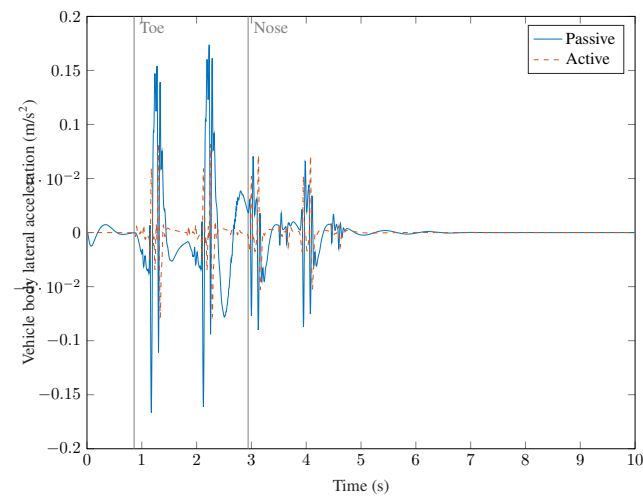

Figure 17. Vehicle body lateral acceleration on the through route of a H switch at v=40 m/s with the 'DIRW 2' controller. The notations 'Active' and 'Passive' used in the graph labels mean the DIRW and conventional vehicles respectively.

Figure 19. Vehicle body lateral acceleration on the diverging route of a H switch at v=40 m/s with the 'DIRW 1' controller. The notations 'Active' and 'Passive' used in the graph labels mean the DIRW and conventional vehicles respectively.
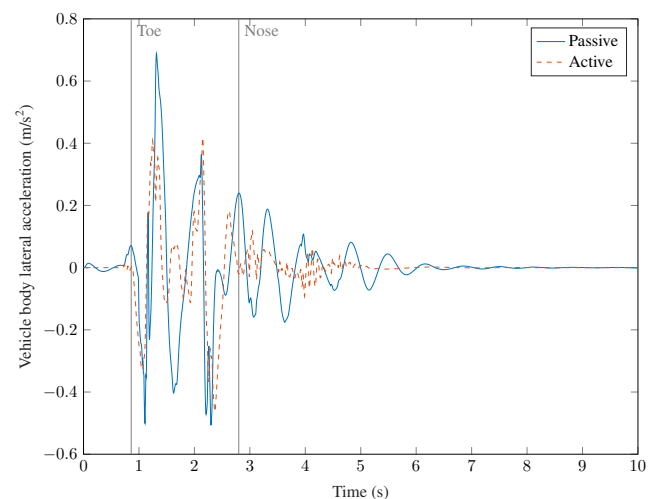
controller. The DIRW vehicle has a much lower lateral displacement at both the toe and the crossing nose than the passive vehicle. The control action also guides it back to the track centreline which is not the case for the passive vehicle which remains displaced by $\approx$2 mm. The vehicle body acceleration is also lower at the toe and nose as shown in Figure 19. These improvements are at the cost of slightly higher longitudinal creep forces generated from the motor torque actuation as shown in Figure 20. The longitudinal creep forces provide a yawing action to the wheelset when it is negotiating the divergence curve. The higher longitudinal creep forces result in significantly higher T_γ values than the passive vehicle as listed in the 'DIRW 1' column in Table 6.

The controller can be optimised to give lower longitudinal creep forces resulting in lower T_γ values at the cost of increased flange contact and increased car body lateral acceleration. With the 'DIRW 1' controller which has the same weightings as through-route scenario, the wheelset

Table 6. T_γ values in J/m on the diverging route of a H switch. The values under 'DIRW 1' column are obtained from simulations with higher controller gains than that in 'DIRW 2' column

	Passive	DIRW 1	DIRW 2
Front bogie front WS	0.5516	3.7864	0.6923
Front bogie rear WS	1.8822	4.8631	2.2861
Rear bogie front WS	0.3218	3.4303	2.2406
Rear bogie rear WS	1.8159	4.0514	2.0841
Total T_γ on all WSs	4.5715	16.1312	7.3031
Percentage of passive	100	352.86	159.75

lateral displacement is lower than with the 'DIRW 2' controller with lower weightings as shown in Figure 21. The car body lateral acceleration is also higher than with the 'DIRW 1' controller but similar to that of the passive vehicle as shown in Figure 22. The longitudinal creep forces are
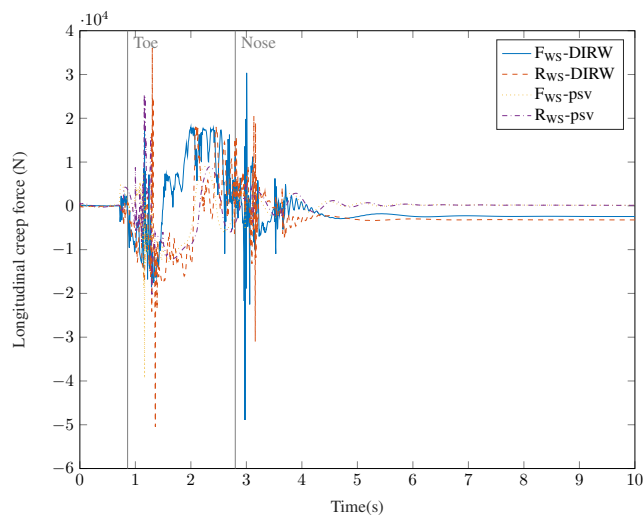
Figure 20. Wheelset longitudinal creep force on the diverging route of a H switch at v=40 m/s with the 'DIRW 1' controller. The notations F_{WS}, R_{WS} and psv used in the graph labels mean 'front wheelset', 'rear wheelset' and 'passive' respectively.

Figure 22. Vehicle body lateral acceleration on the diverging route of a H switch at v=40 m/s with the 'DIRW 2' controller. The notations 'Active' and 'Passive' used in the graph labels mean the DIRW and conventional vehicles respectively.

lower at the nose and on the curve than that in the 'DIRW 1' case as shown in Figure 23 resulting in lower $T\gamma$ values. However, these values indicate that there is more wear than the passive vehicle. Figure 24 shows the $T\gamma$ responses of the passive and DIRW vehicles. From the figure it can be seen that the front wheelset of the passive vehicle has a massive spike just past the toe, whereas the wear is more distributed for both wheelsets of the DIRW vehicle which is better in some aspects.
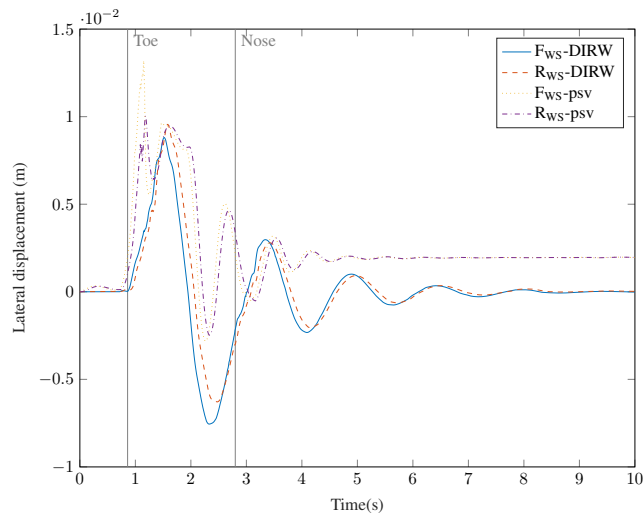

Figure 21. Wheelset lateral displacement on the diverging route of a H switch at v=40 m/s with the 'DIRW 2' controller. The notations F_{WS}, R_{WS} and psv used in the graph labels mean 'front wheelset', 'rear wheelset' and 'passive' respectively.

Figure 23. Wheelset longitudinal creep force on the diverging route of a H switch at v=40 m/s with the 'DIRW 2' controller. The notations F_{WS}, R_{WS} and psv used in the graph labels mean 'front wheelset', 'rear wheelset' and 'passive' respectively.

passive vehicles. On the diverging route the controller can be tuned to achieve different requirements. A lower wheelset lateral displacement and car body lateral acceleration can be achieved at the expense of higher creep forces and wear. So a trade-off may be necessary depending on the objective of the controller. Gain scheduling would also be needed for different switches.

Although this paper looks only at track switch performance, previous work has shown that the DIRW vehicle promises a significant improvement in performance on straight tracks with irregularities and on curved tracks. This suggests that actively-guided vehicles could have a lower wear than passive vehicles across most of the rail network, except perhaps on the divergence routes of high speed track switches. But a higher wear spread across a larger track length may be more desirable than low wear with a large spike.

Conclusions

The results presented in this paper show that an actively-guided vehicle with independently-rotating wheelsets can be used on conventional S&Cs. The active vehicle shows a significant improvement in performance on the through route of low and high speed switches compared to conventional
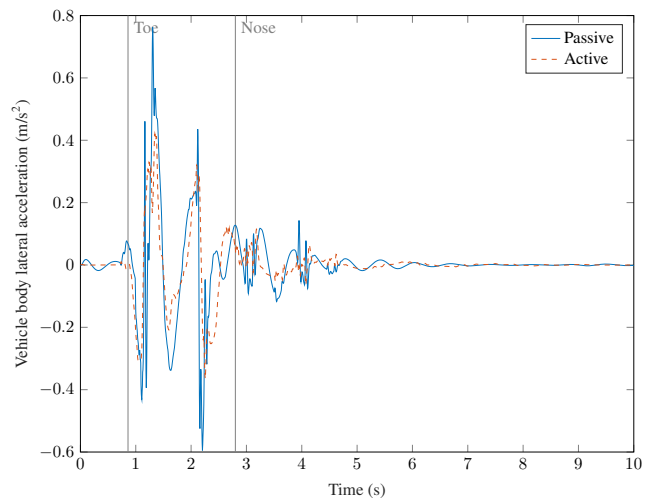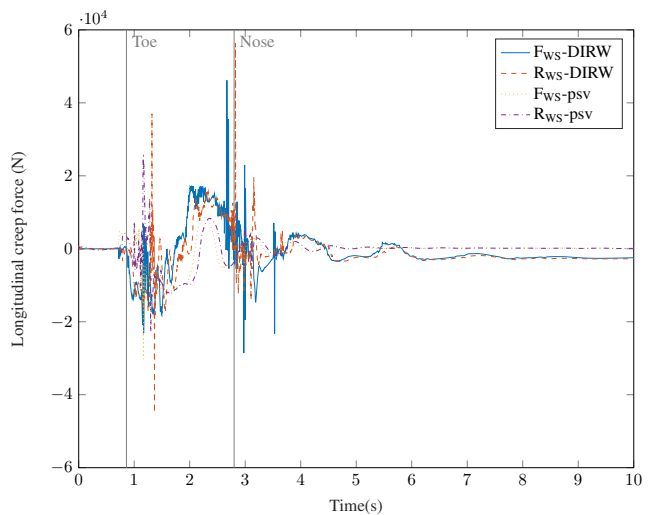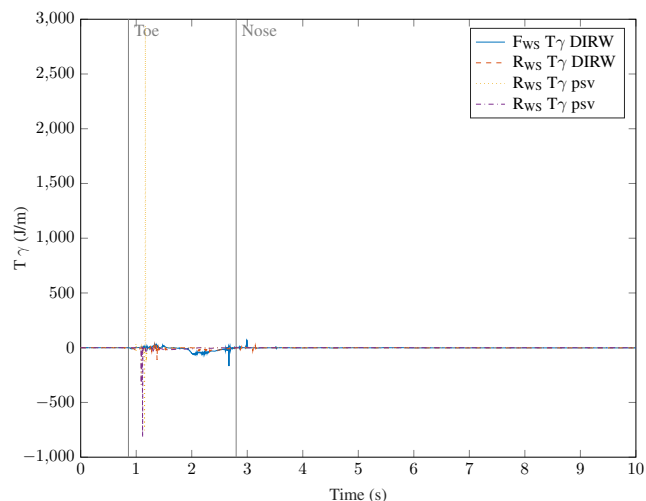
Figure 24. Tγ on the diverging route of a H switch at v=40 m/s with the 'DIRW 2' controller. The notations F_{WS}, R_{WS} and psv used in the graph labels mean 'front wheelset', 'rear wheelset' and 'passive' respectively.

Rail life is dominated by RCF and plastic deformation. Further work is needed to understand these phenomena on IRWs as they are likely to be different than solid-axle wheelsets. Further research will be needed to examine controller strategies that can act fast enough on the diverging route and also to look at passive switches that do not have any moving parts. One way to do this would be to not have the switch rails touching the stock rail on either side of a low speed turnout. The wheel-rail interface at the nose would then be replicated at the toe, therefore introducing the problem of a gap. This is not possible on a high speed turnout with shallow divergence angles, so the exact geometry will need to be researched. The other possibility is to have retractable flanges or even flange-less wheels which would remove the need for gaps at S&Cs.

Acknowledgements

References

Bemment S, Goodall R, Dixon R and Ward C (2017) Improving the reliability and availability of railway track switching by analysing historical failure data and introducing functionally redundant subsystems. *IMechE Part F. JRRT* .

Braghin F, Bruni S and Resta F (2006) Active yaw damper for the improvement of railway vehicle stability and curving performances: simulations and experimental results. *Vehicle System Dynamics* 44(11): 857–869.

Burstow M (2011) Improving track geometry alignment to reduce rolling contact fatigue (rcf). In: *9 World congress on railway research*.

Burstow M (2012) *VTAC calculator: Guidance notes for determining Tγ values*. Network Rail. URL http://www.networkrail.co.uk/cp5-access-charges/guide-to-determining-tgamma-values--vtac-calculator.pdf.

Bushko D, Clark T and Thornton R (2000) Vehicle guidance and switching via magnetic forces. URL https://encrypted.google.com/patents/EP1042152A1?cl=nl. EP Patent App. EP19,980,966,064.

Capacity for Rail C (2015) Operational failure modes of switches and crossings. URL http://www.capacity4rail.eu/IMG/pdf/c4r_-_d131_-_operational_failure_modes_of_scs_public_.pdf. [Online; accessed 04-January-2018].

Caterpillar (2018) Partial flange bearing frog no. 9. URL http://s7d2.scene7.com/is/content/Caterpillar/C10670254. [Online; accessed 04-January-2018].

Dorf RC and Bishop RH (2008) *Modern control systems*. 11 edition. Pearson. ISBN 9780132270281.

Farhat N, Ward CP, Goodall RM and Dixon R (2018) The benefits of mechatronically-guided railway vehicles: A multi-body physics simulation study. *Mechatronics* 51: 115 – 126. DOI:https://doi.org/10.1016/j.mechatronics.2018.03.008. URL http://www.sciencedirect.com/science/article/pii/S0957415818300503.

Goodall R and Ward C (2015) Active control of railway bogies assessment of control strategies. In: *The International Symposium on Speed-up and Sustainable Technology for Railway and Maglev Systems*. Chiba, Japan.

Koseki T, Yang ZP, Ujihara Y and Sone S (2000) On-board turnout in a flexible operation of rail-guided transport system. *IFAC Control in Transportation Systems* 33(9): 535540.

Lindner H (1974) Railway switch for vignoles rails. URL https://www.google.com/patents/US3819935. US Patent 3,819,935.

Mei TX and Goodall RM (2003) Practical Strategies for Controlling Railway Wheelsets Independently Rotating Wheels. *Journal of Dynamic Systems, Measurement, and Control* 125(3): 354–360.

Pearson J, Goodall R, Mei T and Himmelstein G (2004) Active stability control strategies for a high speed bogie. *Control Engineering Practice* 12(11): 1381–1391.

Polach O, Berg M and Iwnicki S (2006) *Handbook of Railway Vehicle dynamics*, chapter Simulation. Taylor & Francis, pp. 360–404.

Rail N (2010) Nr/l2/trk/2049 level 2 track design handbook. Handbook, Network Rail.

Rivington J (1838) Self-acting railway switches.

SET Ltd (2013) Wheelmotor project. URL http://www.set.gb.com/innovation.php. [Online; accessed 23-May-2016].

Standards B (2006) BS EN 13674-2:2006+A1:2010 - Railway applications. Track. Rail. Switch and crossing rails used in conjunction with Vignole railway rails 46 kg/m and above. Standard, British Standards Online.

Standards B (2009) BS EN 12299:2009 - Railway applications - Ride comfort for passengers - Measurement and evaluation. Standard, British Standards Online.

Standards B (2017) BS EN 13674-1:2011+A1:2017 - Railway applications. Track. Rail. Vignole railway rails 46 kg/m and above. Standard, British Standards Online.

Ward CP, Mei TX, Hubbard P and Mirzapour M (2013) Half cost trains: Design for Control. *RRUKA (produced by Loughborough University and University of Salford)* .

Wickens AH (2003) *Fundamentals of Rail Vehicle dynamics, Guidance and Stability*, chapter The bogie vehicle. Swets & Zeitlinger, Lisse, Netherlands, p. 174.

Wu H and Wilson N (2006) *Handbook of Railway Vehicle dynamics*, chapter Railway vehicle derailment and prevention. Taylor & Francis, pp. 214–216.

Young P, Behzadi MA, Wang CL and Chotai A (1987) Direct digital and adaptive control by input-output state variable feedback pole assignment. *International Journal of Control* 46(6): 1867–1881. DOI:10.1080/00207178708934021. URL https://doi.org/10.1080/00207178708934021.

Yusof H, Goodall RM and Dixon R (2011) Controller strategies for active secondary suspension actuators. In: *22nd International Symposium on Dynamics of Vehicles on Roads and Tracks*. URL http://eprints.hud.ac.uk/id/eprint/17752/. IAVSD2011 Symposium Proceedings CD (ISBN 9781905476596).